International Journal of Mechanical Sciences 57 (2012) 9–18

Contents lists available at SciVerse ScienceDirect

International Journal of Mechanical Sciences

journal homepage: www.elsevier.com/locate/ijmecsci

Multi-linear stress–strain and closed-form moment curvature response of epoxy resin materials

Masoud Yekani Fard*, Aditi Chattopadhyay, Yingtao Liu

Department of Mechanical and Aerospace Engineering, School of Engineering of Matter, Transport and Energy, Arizona State University, Tempe, AZ 85287-6106, USA

ARTICLE INFO

Article history:
Received 14 May 2010
Received in revised form
6 January 2012
Accepted 9 January 2012
Available online 28 January 2012

Keywords:
Epoxy resins
Stress–strain relation
Moment curvature
Nonlinear behavior
Load deflection
Flexural response

ABSTRACT

A simplified multi-linear stress–strain approach has been used to obtain the closed form nonlinear moment curvature response for epoxy resin materials. The model consists of constant plastic flow in tension and compression. The multi-linear stress–strain model is described by two main parameters in addition to four non-dimensional tensile and six non-dimensional compressive parameters. The main parameters are modulus of elasticity in tension and strain at the proportional elastic limit point in tension. The ten non-dimensional parameters are strain at the ultimate tensile stress, maximum strain, post elastic proportionality stiffness, and post peak strength in the tension model and strain at the proportionality elastic limit, strain at yield strength point, maximum strain, initial elastic stiffness, post elastic proportionality stiffness, and post peak strength in the compression model. Explicit expressions are derived for the stress–strain behavior of the epoxy resins. Closed form equations for moment curvature relationship are presented. The results of tension, compression, and bending tests using digital image correlation technique are presented. Load deflection response of flexural three point bending (3PB) samples could be predicted using the moment curvature equations, crack localization rules, and fundamental static equations. The simulations and experiments reveal that the direct use of uniaxial tensile and compressive stress–strain curves underestimates the flexural response. This model gives an upper bound estimate for flexural over-strength factor.

1. Introduction

Epoxy resins are one of the frequent matrix materials in fiber composites. Mechanical properties (stress–strain relationship) and progressive failure is still a challenge for researchers. Difficulty of a constitutive law in polymer matrix composites is mainly due to the characterization of polymer mechanical behavior. The hydrostatic component of stress has a significant effect on the load deformation response of resins even at low levels of stress. Hydrostatic stresses are known to affect the yield stress of polymers; the absolute value of the yield stress in compression is higher than the ultimate tensile stress. In order to develop a general model for polymer composite materials, the behavior of polymer resins under different types of loading has to be understood. Wineman and Rajagopal [1] used a viscoplasticity model to capture the polymer behavior. Zhang and Moore [2] used the Bodner–Partom internal state variable model originally developed for metals to obtain the nonlinear uniaxial tensile response of polyethylene. By modifying the definitions of the effective stress and effective inelastic strain rate in the Drucker–Prager yield criteria, Li and Pan [3], Chang and Pan [4], and Hsu et al. [5] developed a viscoplasticity approach for the constitutive law of polymer materials. Gilat et al. [6] used an internal state variable model to modify the Bodner model to capture the effects of hydrostatic stresses on the response. In their approach, a single unified strain variable is defined to represent all inelastic strains. Jordan et al. [7] modified the original Mulliken–Boyce model [8] for one dimension to capture the compressive mechanical properties of polymer composites. The original model is a three dimensional strain rate and temperature dependent model for thermoplastic polymers. The majority of the parameters were determined by fitting the model to experimental compressive data. A piecewise-linear tension and compression stress–strain relationship was used to study the mechanical behavior of high performance fiber-reinforced cement composites [9]. Yekani Fard et al. [10,11] studied the nonlinear mechanical behavior of Epon E 863 using the Digital Image Correlation (DIC) system. Hobbiebrunken et al. [12], Bazant and Chen [13], Odom and Adam [14], and Goodier [15] studied the dependency of the failure and strength on the size effect, stress state, and volume of the body subjected to stress in epoxy resin polymers. Giannotti et al. [16] and Vallo [17] used the statistical Weibull analysis approach and estimated the mean flexural strength to be 40% higher than the tensile strength for a Weibull modulus greater than 14.

* Corresponding author. Tel.: +1 480 370 9786; fax: +1 480 727 9321.
E-mail address: masoud.yekanifard@asu.edu (M. Yekani Fard).

0020-7403/$ - see front matter © 2012 Elsevier Ltd. All rights reserved.
doi:10.1016/j.ijmecsci.2012.01.009

Yekani Fard et al. [18,19] used an analytical approach to evaluate the flexural over-strength factor in epoxy resin E 863. They observed that the flexural strength in 3PB beams with groove was at least 14% higher than the tensile peak stress at low strain rates. Flexural over-strength factor is the ratio of the flexural strength (peak stress) to the ultimate tensile strength (UTS).

In this study, the flexural behavior of a beam is investigated in an attempt to establish a relationship between the tensile and compressive stress–strain curves (with constant plastic flow) in one side and moment curvature response of epoxy resin material in the other side. In order to correlate tension, compression stress–strain curves and flexural data, a closed form solution has been developed to obtain moment curvature response. The load deflection response for nonlinear materials under determinate static conditions has been developed. Using inverse analysis, the effect of stress gradient on the multi-linear stress–strain curve obtained from the in-plane uniaxial tests has been studied.

2. Tension and compression multi-linear stress–strain curve

The multi-linear stress–strain curve for tension and compression is bilinear up to the peak stress. Fig. 1 shows the tension and compression stress–strain relationship of epoxy resin materials. The tension and compression curves are defined uniquely by the parameters E, ε_{PEL}, μ_{t1}, μ_{Ut},α, ω, γ, β, ψ, μ_{co}, μ_{c1}, and μ_{Uc}. The tensile stress at the proportionality elastic point (PEL) is related empirically to the stress at the ultimate tensile strength (UTS) point. The ascending part of the tension and compression stress–strain diagrams consist of two linear parts: 0 to PEL, and PEL to UTS in tension or PEL to compressive yield stress (CYS) in compression. The curve after peak strength is idealized as horizontal with σ_{ft} and σ_{fc} as the post peak sustained stress in tension and compression respectively. The constant post peak stress levels (ω and ψ) shows the ability of the model to represent a continuous ($\omega=\psi=1$) or discontinuous stress response. The post peak response in tension terminates at the ultimate tension strain level ($\varepsilon_{Ut}=\mu_{Ut}\,\varepsilon_{PEL}$), and for compression it ends at ultimate compression strain level ($\varepsilon_{Uc}=\mu_{Uc}\,\varepsilon_{PEL}$). In the elastic range, the resin beam in bending could be treated as a bi-modulus material with different moduli in tension and compression. The tension and compression stress–strain relationship are defined as shown in Table 1.

σ_c, σ_t, ε_c, and ε_t are compression and tension stresses and strains, respectively. The ten normalized parameters used in the definition of the constitutive law are defined by

$$\mu_{c0}=\frac{\varepsilon_{PEL,c}}{\varepsilon_{PEL}},\ \mu_{c1}=\frac{\varepsilon_{CYS}}{\varepsilon_{PEL}},\ \mu_{Uc}=\frac{\varepsilon_{Uc}}{\varepsilon_{PEL}},\ \mu_{t1}=\frac{\varepsilon_{Uts}}{\varepsilon_{PEL}},\ \mu_{Ut}=\frac{\varepsilon_{Ut}}{\varepsilon_{PEL}} \tag{1}$$

$$\gamma=\frac{E_c}{E},\ \beta=\frac{E_{PEL,c}}{E},\ \alpha=\frac{E_{PEL,t}}{E} \tag{2}$$

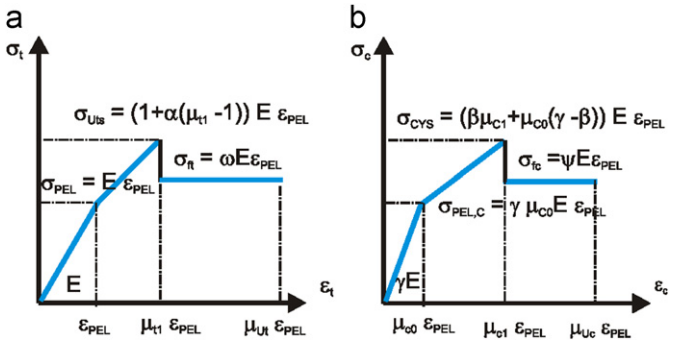

Fig. 1. (a) Constant flow in tension; (b) constant flow in compression.

Table 1
Multi-linear stress–strain curve.

Stress	Definition	Domain of strain
$\sigma_t(\varepsilon_t)$	$E\varepsilon_t$	$0\le\varepsilon_t\le\varepsilon_{PEL}$
	$E(\varepsilon_{PEL}+\alpha\,(\varepsilon_t-\varepsilon_{PEL}))$	$\varepsilon_{PEL}<\varepsilon_t\le\mu_{t1}\,\varepsilon_{PEL}$
	$\omega\,E\,\varepsilon_{PEL}$	$\mu_{t1}\,\varepsilon_{PEL}<\varepsilon_t\le\mu_{Ut}\,\varepsilon_{PEL}$
	0	$\mu_{Ut}\,\varepsilon_{PEL}<\varepsilon_t$
$\sigma_c(\varepsilon_c)$	$\gamma\,E\,\varepsilon_c$	$0\le\varepsilon_c\le\mu_{c0}\,\varepsilon_{PEL}$
	$E\,(\gamma\,\mu_{c0}\,\varepsilon_{PEL}+\beta\,(\varepsilon_c-\mu_{c0}\,\varepsilon_{PEL}))$	$\mu_{c0}\,\varepsilon_{PEL}<\varepsilon_c\le\mu_{c1}\,\varepsilon_{PEL}$
	$\psi\,E\,\varepsilon_{PEL}$	$\mu_{c1}\,\varepsilon_{PEL}<\varepsilon_c\le\mu_{Uc}\,\varepsilon_{PEL}$
	0	$\mu_{Uc}\,\varepsilon_{PEL}<\varepsilon_c$

$$\omega=\frac{\sigma_{ft}}{\sigma_{PEL}},\ \psi=\frac{\sigma_{fc}}{\sigma_{PEL}} \tag{3}$$

Using classical beam theory, linear distribution of strain across the depth is assumed. The stress and strain distribution across a section of a beam with depth h and width b by imposing normalized top compressive strain in different cases are shown in Fig. 2. Normalized heights of compression and tension sub-zones with respect to beam depth h are shown in Table 2. Tables 3 and 4 present the normalized stress at the vertices of the tension and compression sub-zones with respect to tensile stress at the proportionality limit point. The internal force in each compression and tension sub-zone of nine stress distribution cases could be calculated from the stress diagram. The centroid of the stress in each sub-zone represents the line of action and moment arm respect to the neutral axis.

3. Closed-form moment curvature response

The development of stress–strain across the section by increasing the normalized compressive strain is presented in Fig. 3. Stress–strain develops at least to stage 4 where compressive and tensile failure is possible if $\lambda_{max}=\mu_{Uc}$ in case 6, or $\lambda_{max}=F$ in case 4. Moving through different stages in Fig. 3 depends on the controlling value for λ_{max}. Using the auxiliary points defined in Table 5, the transition points defined as tp_{ij} between different stages in Fig. 3 could be presented by the following equations.

$$\begin{aligned}
&tp_{12}=Min(\mu_{c0},A)\\
&tp_{23}=Min(\mu_{c0},C)\ or\ Min(\mu_{c1},B)\\
&tp_{34}=Min(\mu_{Uc},D)\ or\ Min(\mu_{c1},E)\ or\ Min(\mu_{c0},F)\\
&tp_{45}=Min(\mu_{Uc},G)\ or\ Min(\mu_{c1},H)\\
&tp_{56}=Min(\mu_{Uc},I)
\end{aligned} \tag{4}$$

where indexes i and j refer to origin and destination stages, respectively. The net force is obtained as the difference between the tension and compression forces, equated to zero for internal equilibrium, and solved for the neutral axis depth ratio defined as κ. The expressions of net force in some stages result in more than one solution for κ. Using a large scale of numerical tests covering possible ranges of material parameters, the solution of κ which yields the valid value $0<\kappa<1$ was determined and presented in Table 6. Moment expressions are obtained by taking the first moment of the compression and tension forces about the neutral axis. Curvature is calculated by dividing the top compressive strain by the depth of the neutral axis κh. The closed form solutions for normalized moment M_i and curvature φ_i with respect to the values at the tensile PEL points are presented in Eqs. (5)–(7) and Table 6.

$$M=M_{PEL}M'(\lambda,\gamma,\beta,\alpha,\mu_{c0},\mu_{c1},\mu_{t1},\mu_{Ut},\mu_{Uc},\omega,\psi) \tag{5}$$

$$\varphi=\varphi_{PEL}\varphi'(\lambda,\gamma,\beta,\alpha,\mu_{c0},\mu_{c1},\mu_{t1},\mu_{Ut},\mu_{Uc},\omega,\psi) \tag{6}$$

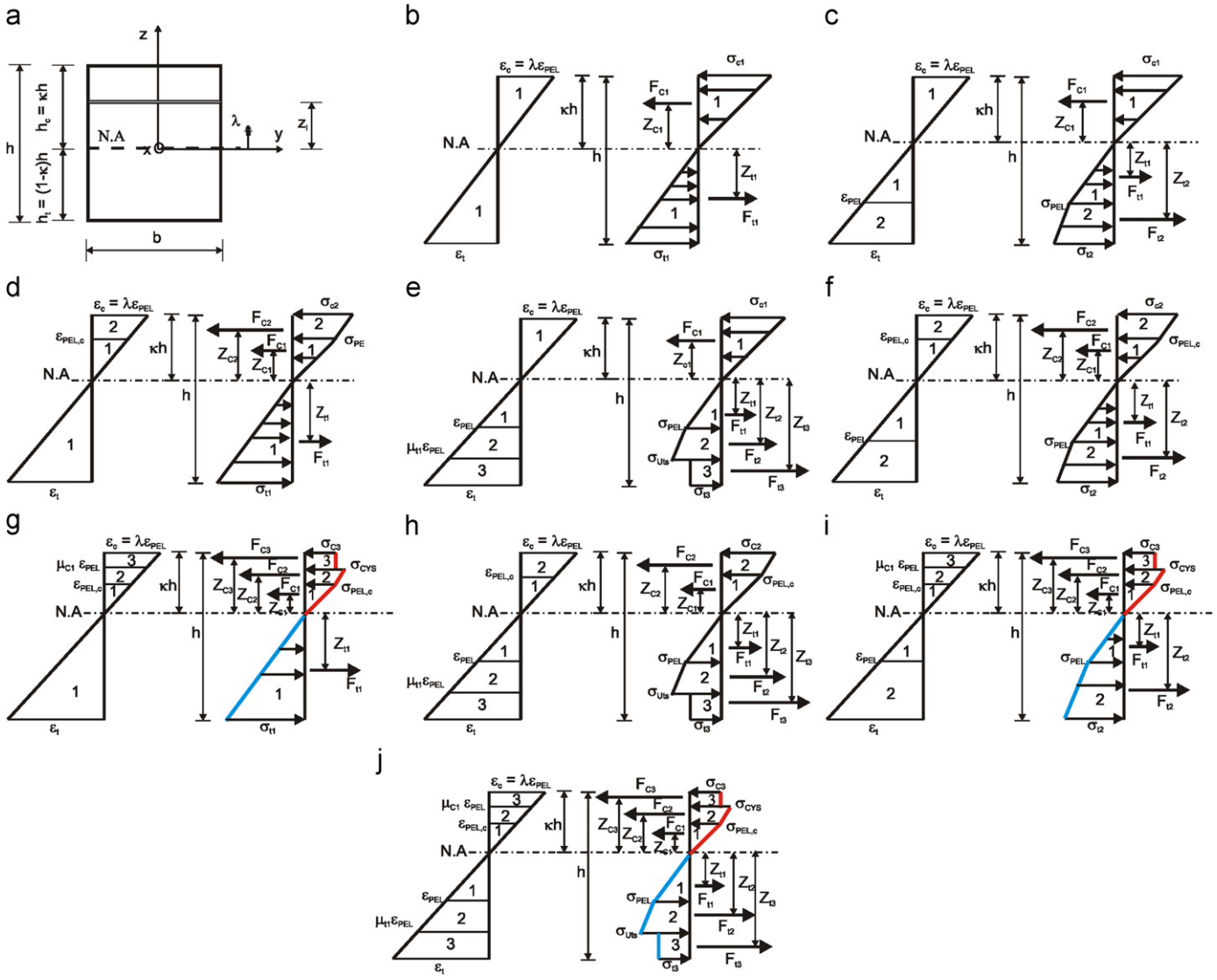

Fig. 2. (a) Rectangular cross section, (b) to (j) stress–strain distributions across the cross section for cases 1 to 9, respectively.

Table 2
Normalized height of tension and compression sub zone for each case.

Cases	$\frac{h_{c3}}{h}$	$\frac{h_{c2}}{h}$	$\frac{h_{c1}}{h}$	$\frac{h_{t1}}{h}$	$\frac{h_{t2}}{h}$	$\frac{h_{t3}}{h}$
1,3,6	–	–	–	$(1-\kappa)$	–	–
2,5,8	–	–	–	$\frac{\kappa}{\lambda}$	$1-\kappa-\frac{\kappa}{\lambda}$	–
4,7,9	–	–	–	$\frac{\kappa}{\lambda}$	$\frac{\kappa}{\lambda}(\mu_{t1}-1)$	$1-\kappa-\frac{\mu_{t1}\kappa}{\lambda}$
1,2,4	–	–	κ	–	–	–
3,5,7	–	$\kappa\left(1-\frac{\mu_{c0}}{\lambda}\right)$	$\frac{\mu_{c0}\kappa}{\lambda}$	–	-	–
6,8,9	$\kappa\left(1-\frac{\mu_{c1}}{\lambda}\right)$	$\frac{\kappa}{\lambda}(\mu_{c1}-\mu_{c0})$	$\frac{\mu_{c0}\kappa}{\lambda}$	–	–	–

$$\varphi'_i(\lambda,\gamma,\beta,\alpha,\mu_{c0},\mu_{c1},\mu_{t1},\mu_{Ut},\mu_{Uc},\omega,\psi) = \frac{\lambda}{2\kappa_i},\ i = 1,2,3,\ldots,9 \tag{7}$$

where M_{PEL} and φ_{PEL} are elastic moment and curvature and are defined as

$$M_{PEL} = \frac{bh^2 E\varepsilon_{PEL}}{6},\ \varphi_{PEL} = \frac{2\varepsilon_{PEL}}{h} \tag{8}$$

The ultimate moment M_u (flexural strength) is computed based on Eqs. (5) and (8) and Table 6. For a material like resin, M_u could approach M_∞ at very large λ values. The normalized moment at the very large λ values M'_∞ is computed by substituting $\lambda=\infty$ in the expression for κ in case nine of Table 6 and by substitution of $\lambda=\infty$ and κ_∞ in the normalized moment expression. Eqs. (9)–(11) present the values of the neutral axis depth,

Table 3
Normalized stress at vertices of each tension sub zone for each case.

Cases	$\frac{\sigma_{t1}}{E\varepsilon_{PEL}}$	$\frac{\sigma_{t2}}{E\varepsilon_{PEL}}$	$\frac{\sigma_{t3}}{E\varepsilon_{PEL}}$
1,3,6	$\left(\frac{1-\kappa}{\kappa}\right)\lambda$	–	–
2,5,8	1	$1+\alpha\left(\frac{(1-\kappa)\lambda}{\kappa}-1\right)$	–
4,7,9	1	$1+\alpha(\mu_{t1}-1)$	ω

Table 4
Normalized stress at vertices of each compression sub zone for each case.

Cases	$\frac{\sigma_{c3}}{E\varepsilon_{PEL}}$	$\frac{\sigma_{c2}}{E\varepsilon_{PEL}}$	$\frac{\sigma_{c1}}{E\varepsilon_{PEL}}$
1,2,4	–	–	$\gamma\lambda$
3,5,7	–	$\gamma\mu_{c0}+\beta(\lambda-\mu_{c0})$	$\gamma\mu_{c0}$
6,8,9	ψ	$\gamma\mu_{c0}+\beta(\mu_{c1}-\mu_{c0})$	$\gamma\mu_{c0}$

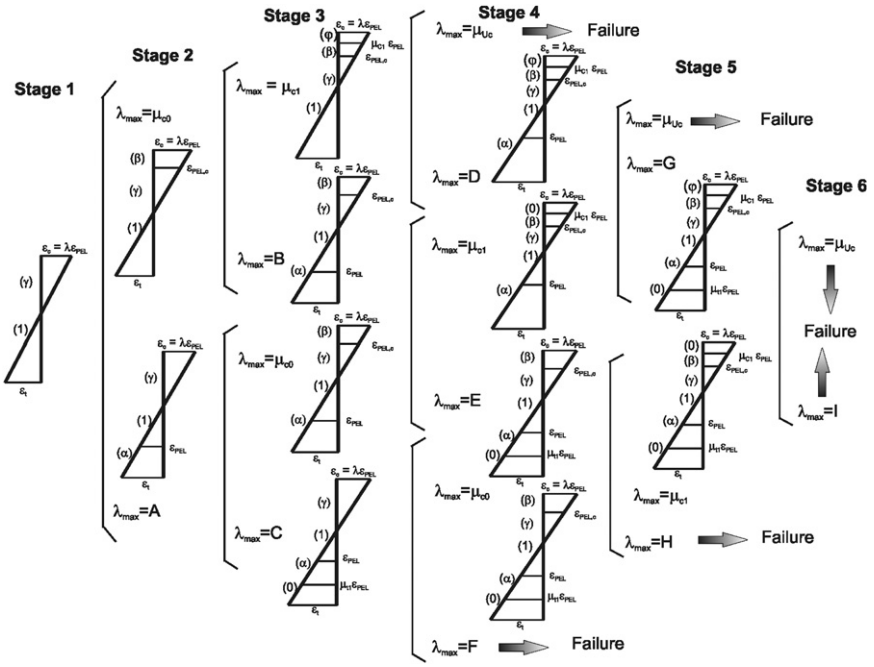

Fig. 3. Strain development in the cross section at different stages of loading.

Table 5
Auxiliary transition points in the stress–strain development diagram.

A(γ)	$\frac{\sqrt{\gamma}-1}{\gamma-\sqrt{\gamma}}$
B(γ,β,μ_{c0})	$\frac{\mu_{c0}(\beta-\gamma)+\sqrt{\mu_{c0}^2\gamma(\gamma-\beta)+\beta}}{\beta}$
C(γ,α,μ_{t1})	$\sqrt{\frac{\alpha(\mu_{t1}-1)^2+2\mu_{t1}-1}{\gamma}}$
D(γ,β,μ_{c0},μ_{c1})	$\frac{1+(\gamma-\beta)(\mu_{c1}-\mu_{c0})^2-\gamma\mu_{c1}^2+2\psi\mu_{c1}}{2\psi}$
E(γ,β,μ_{c0},α,μ_{t1})	$\frac{\mu_{c0}(\beta-\gamma)+\sqrt{\gamma\mu_{c0}^2(\gamma-\beta)+\alpha\beta\mu_{t1}^2+\beta(1-\alpha)(2\mu_{t1}-1)}}{\beta}$
F(γ,α,μ_{t1},μ_{Ut},ω)	$\sqrt{\frac{2\omega(\mu_{Ut}-\mu_{t1})+\alpha(\mu_{t1}-1)^2+2\mu_{t1}-1}{\gamma}}$
G(γ,β,μ_{c0},μ_{c1},α,μ_{t1})	$\frac{(\gamma-\beta)(\mu_{c1}-\mu_{c0})^2+\alpha(\mu_{t1}-1)^2+2\psi\mu_{c1}-\gamma\mu_{c1}^2+2\mu_{t1}-1}{2\psi}$
H(γ,β,μ_{c0},α,μ_{t1},μ_{Ut},ω)	$\frac{\mu_{c0}(\beta-\gamma)+\sqrt{2\omega\beta(\mu_{Ut}-\mu_{t1})+\gamma\mu_{c0}^2(\gamma-\beta)+\alpha\beta\mu_{t1}^2+\beta(1-\alpha)(2\mu_{t1}-1)}}{\beta}$
I(γ,β,μ_{c0},μ_{c1},α,μ_{t1},μ_{Ut},ω)	$\frac{2\omega\mu_{Ut}+\alpha(\mu_{t1}-1)^2-1-2\mu_{t1}(\omega-1)+2\psi\mu_{c1}-\gamma\mu_{c1}^2+(\gamma-\beta)(\mu_{c1}-\mu_{c0})^2}{2\psi}$

normalized moment, and curvature for very large λ values.

$$\kappa_\infty = \frac{\omega}{\omega+\psi} \tag{9}$$

$$M'_\infty = \frac{3\omega\psi}{\omega+\psi} \tag{10}$$

$$\varphi'_\infty = \infty \tag{11}$$

The neutral axis depth and normalized moment for very large strain values are a function of post peak tension and compression strengths. For an elastic perfectly plastic materials with equal tensile and compression elastic moduli and equal yield and post peak flow stress, Eqs. (9) and (10) yields to 0.5 and 1.5, respectively, validating the theoretical value that the plastic moment capacity of a rectangular section is 1.5 times its elastic yield strength presented by Salmon [20]. The critical value of ω which results in a flexural capacity in the infinity (before failure) greater than the flexural capacity at the tensile PEL point is expressed as

$$\omega_{critical} = \frac{\psi}{3\psi-1} \tag{12}$$

4. Parametric study

Parametric studies determine the sensitivity of the different parts of the model to the relative behavior of the variables. Effect of the tension and compression stress–strain relation on the response of polymer materials was addressed by studying the effect of variation of a parameter in the constitutive law while all other parameters were held constant to the typical values. Epon E 862 epoxy resin was chosen and typical mechanical characteristic of E 862 are E=2069 MPa, Ec=2457 MPa, ε_{PEL}=0.0205, ε_{Uts}=0.076, ε_{Ut}=0.24, $\varepsilon_{PEL,c}$=0.019, ε_{CYS}=0.092, ε_{Uc}=0.35, σ_{Uts}=70 MPa, σ_{ft}=60.5 MPa, σ_{fc}=83 MPa, σ_{CYS}=93 MPa [21]. The flexural strength and ductility for each material parameter was expressed as the normalized moment curvature response, independent of geometry and tensile PEL strength.

4.1. Strain softening in tension

Fig. 4 shows the results of the parametric study for strain softening material. Fig. 4(a1)–(a3) presents the effect of constant flow tensile strength on the moment curvature and on the location of neutral axis depth. ω=0.017 and 1.63 correspond to constant tensile plastic flow equal to 1% and 100% of the ultimate tensile strength respectively. Fig. 4(a2) depicts that moment curvature response is extremely sensitive to the variations in constant tensile flow as the location of maximum flexure and the post peak regime completely changes withω. The flexural response changes from brittle to ductile behavior as ω increases from 0.017 to 1.63. When ω=1.42 the response characterizes exactly the material behavior of Epon E 862, and Eq. (10) gives $M'_\infty = 2.58$ as it can be seen from Fig. 4(a2). Fig. 4(a3) shows that decreasing the level of tensile flow decreases the neutral axis depth, especially for ω values less than 0.5 (30% of UTS). Tensile failure was the governing mechanism in all the material responses. Materials with ω=0.08 and ω=0.017 did not experience compression yield and their stress–strain relationship always were in the elastic compression region. This is the reason that their neutral axis depth and moment capacity drops sharply

Table 6
Neutral axis depth ratio, and moment for each case.

Case	κ_i	M_i'
1	$\frac{-1+\sqrt{\gamma}}{\gamma-1}$	$2\lambda(\gamma-1)\kappa_1^2+6\lambda\kappa_1-6\lambda+\frac{2\lambda}{\kappa_1}$
2	$\frac{-\lambda(\alpha(\lambda+1)-1-\sqrt{-\alpha+1+\alpha\gamma\lambda^2})}{-t_1+\gamma\lambda^2}$, $t_1=\alpha(\lambda+1)^2-2\lambda-1$	$\frac{((1-\alpha)(3\lambda^2-1)-2\lambda^3(\alpha-\gamma))\kappa_2^2}{\lambda^2}+t_9\kappa_2+t_{10}+\frac{2\alpha\lambda}{\kappa_2}$, $t_9=6(\alpha(\lambda+1)-1)$, $t_{10}=3(1-\alpha(1+2\lambda))$
3	$\frac{\lambda(\lambda-\sqrt{t_2})}{\lambda^2-t_2}$, $t_2=(\lambda-\mu_{c0})^2(\beta-\gamma)+\gamma\lambda^2$	$\frac{(t_5-2\lambda^3(1-\beta))\kappa_3^2}{\lambda^2}+6\lambda(\kappa_3-1)+\frac{2\lambda}{\kappa_3}$, $t_5=(\beta-\gamma)\mu_{c0}(\mu_{c0}^2-3\lambda^2)$
4	$\frac{2\omega\lambda}{t_4+\gamma\lambda^2}$, $t_4=1+2\omega\lambda+2\mu_{t1}(\omega-1)-\alpha(\mu_{t1}-1)^2$	$\frac{(t_7+t_8+2(\gamma\lambda^3+\alpha\mu_{t1}^3))\kappa_4^2}{\lambda^2}-6\omega\kappa_4+3\omega$, $t_7=(1-\alpha)(3\mu_{t1}^2-1)$, $t_8=3\omega(\lambda^2-\mu_{t1}^2)$
5	$\frac{\lambda(\alpha(\lambda+1)-1-\sqrt{-\alpha+1+\alpha t_2})}{t_1-t_2}$	$\frac{(t_5-2\lambda^3(\alpha-\beta)+(1-\alpha)(3\lambda^2-1))\kappa_5^2}{\lambda^2}+t_9\kappa_5+t_{10}+\frac{2\alpha\lambda}{\kappa_5}$
6	$\frac{\lambda(\lambda-\sqrt{t_3})}{\lambda^2-t_3}$, $t_3=(\beta-\gamma)(\mu_{c1}-\mu_{c0})^2+\gamma\mu_{c1}^2-2\psi(\mu_{c1}-\lambda)$	$\frac{(t_6-2\lambda^3)\kappa_6^2}{\lambda^2}+6\lambda(\kappa_6-1)+\frac{2\lambda}{\kappa_6}$, $t_6=\mu_{c0}(\beta-\gamma)(\mu_{c0}^2-3\mu_{c1}^2)+2\beta\mu_{c1}^3+3\psi(\lambda^2-\mu_{c1}^2)$
7	$\frac{2\omega\lambda}{t_4+t_2}$	$\frac{(t_5+t_7+t_8+2(\beta\lambda^3+\alpha\mu_{t1}^3))\kappa_7^2}{\lambda^2}-6\omega\kappa_7+3\omega$
8	$\frac{\lambda(\alpha(\lambda+1)-1-\sqrt{-\alpha+1+\alpha t_3})}{t_1-t_3}$	$\frac{(t_6+3\lambda^2(1-\alpha)+\alpha(1-2\lambda^3)-1)\kappa_8^2}{\lambda^2}+t_9\kappa_8+t_{10}+\frac{2\alpha\lambda}{\kappa_8}$
9	$\frac{2\omega\lambda}{t_4+t_3}$	$\frac{(t_6-3\mu_{t1}^2(\omega+\alpha-1)+\alpha(1+2\mu_{t1}^3)+3\omega\lambda^2)\kappa_9^2}{\lambda^2}-6\omega\kappa_9+3\omega$

by applying top compressive strain, and they show a brittle material behavior.

4.2. Ultimate tensile strength

Fig. 4(b1)–(b3) depicts the effect of UTS on the moment curvature and neutral axis location at constant tensile post PEL slope and constant tensile flow stress. Fig. 4(b2) reveals that an increase in μ_{t1}, increases flexural strength and this is clear for high μ_{t1} values. However, the amount of M_∞' is not affected as much as the flexural strength since for $\mu_{t1}>6$ the moment at infinity is less than the flexural strength. Fig. 4(b3) shows that by increasing the ultimate tensile strength, neutral axis moves downward and approaches toward $\kappa=0.5$. One can look at the variation of μ_{t1} as the variation of CYS to UTS ratio which is defined as $\frac{\gamma\mu_{c0}+\beta(\mu_{c1}-\mu_{c0})}{1+\alpha(\mu_{t1}-1)}$ and by substituting $\gamma=1.19$, $\beta=0.3$, $\alpha=0.24$, $\mu_{c0}=0.93$, $\mu_{c1}=4.49$, it is clear that changes in μ_{t1} from 2.75 to 8 will change the CYS to UTS ratio from 1.53 to 0.81.

4.3. Post PEL slope in tension

Fig. 4(c1) shows the compression and tension model with the post tensile PEL slope and strain of UTS points varied from 0.15 to 0.6, and 5.33 to 2.083 respectively, at fixed UTS and post peak tensile flow. Stress–strain models of three sets of α and μ_{t1} are shown in Fig. 4(c1). Fig. 4(c2) and (c3) reveal that changes in parameters α and μ_{t1} slightly affect the moment but extremely affect position of the neutral axis for a wide range of normalized top compressive strains between 1 and 4 and that will change the stress distribution across the section between elastic and post peak range.

4.4. Post PEL slope in compression

In order to study the effect of post compressive PEL stiffness, the range of parameters β and μ_{c1} were used to represent the variation in β while CYS was constant. The compressive and tensile stress–strain models are shown in Fig. 4(d1). Unlike the post tensile PEL stiffness, analyses of Fig. 4(d2) depicts that flexural strength is quite sensitive to the large variations in parameter β as it significantly affects the flexural strength. Increasing β and decreasing μ_{c1} slightly affect the ductility as it is shown in Fig. 4(d2). Fig. 4(d3) shows the profile of the neutral axis position versus the applied top compressive strain. Curves of ($\beta=0.1$, $\mu_{c1}=11.61$) and ($\beta=0.2$, $\mu_{c1}=6.27$) have completely different shape comparing to others. After λ exceeds the compressive PEL, the neutral axis depth increases sharply to statically equilibrate the axial forces in the cross section but since CYS is greater than UTS and tensile plastic flow, it starts to decrease in post peak regions. Material with ($\beta=0.1$, $\mu_{c1}=11.61$) did not experience any yield in compression and all are failed in tension.

4.5. Compressive yield stress

Fig. 4(e1) shows the compressive and tensile stress–strain relationship with different β and constant μ_{c1}. Increasing the compressive yield strength increases the flexural capacity as it is shown by the normalized moment curvature plots in Fig. 4(e2). Analyses indicate that tension is the governing failure mechanism in all cases while compression strain exceeds the yield point.

4.6. Initial elastic stiffness in compression

In order to study the effect of initial compressive stiffness, a range of parameters, γ and μ_{c0}, were coupled to represent the increase in relative compressive to tensile stiffness from 0.8 to 1.4 at a fixed compressive PEL to tensile PEL ratio of $\gamma\mu_{c0}=1.107$ as shown in Fig. 4(f1). Fig. 4(f2) and (f3) reveal that changes in the relative stiffness slightly affect the moment curvature and the location of the neutral axis especially in the nonlinear phase. Analyses show that all the cases experience yielding in compression and failure in tension.

5. Load deflection relationship

When a beam is loaded beyond the load carrying capacity (Modulus of Rupture, MOR) in a material with deflection softening behavior, increase the deformation decreases load in the distinct zone (around the loading nose in 3PB) in the cracking region while

the rest of the beam undergoes unloading. The length of the localized zone in 3PB with groove with the length of 60 mm, obtained from strain field analysis, is 5 mm at 493 μstr/s as shown in Fig. 5. Moment distribution along the beam is obtained through the static equilibrium of the beam, and the curvature of each point along the beam is obtained though the moment curvature diagram. In order to obtain the load deflection response for 3PB from the moment curvature diagram, an array of discrete load steps is defined for a given moment curvature diagram using static equilibrium. The specimen is loaded from 0 to P_{max} in the ascending portion of the moment curvature diagram from 0 to M_{max}. The curvature for this portion is determined directly from the moment curvature diagram. Once the moment reaches MOR, the curvature distribution along the beam in the softening regime

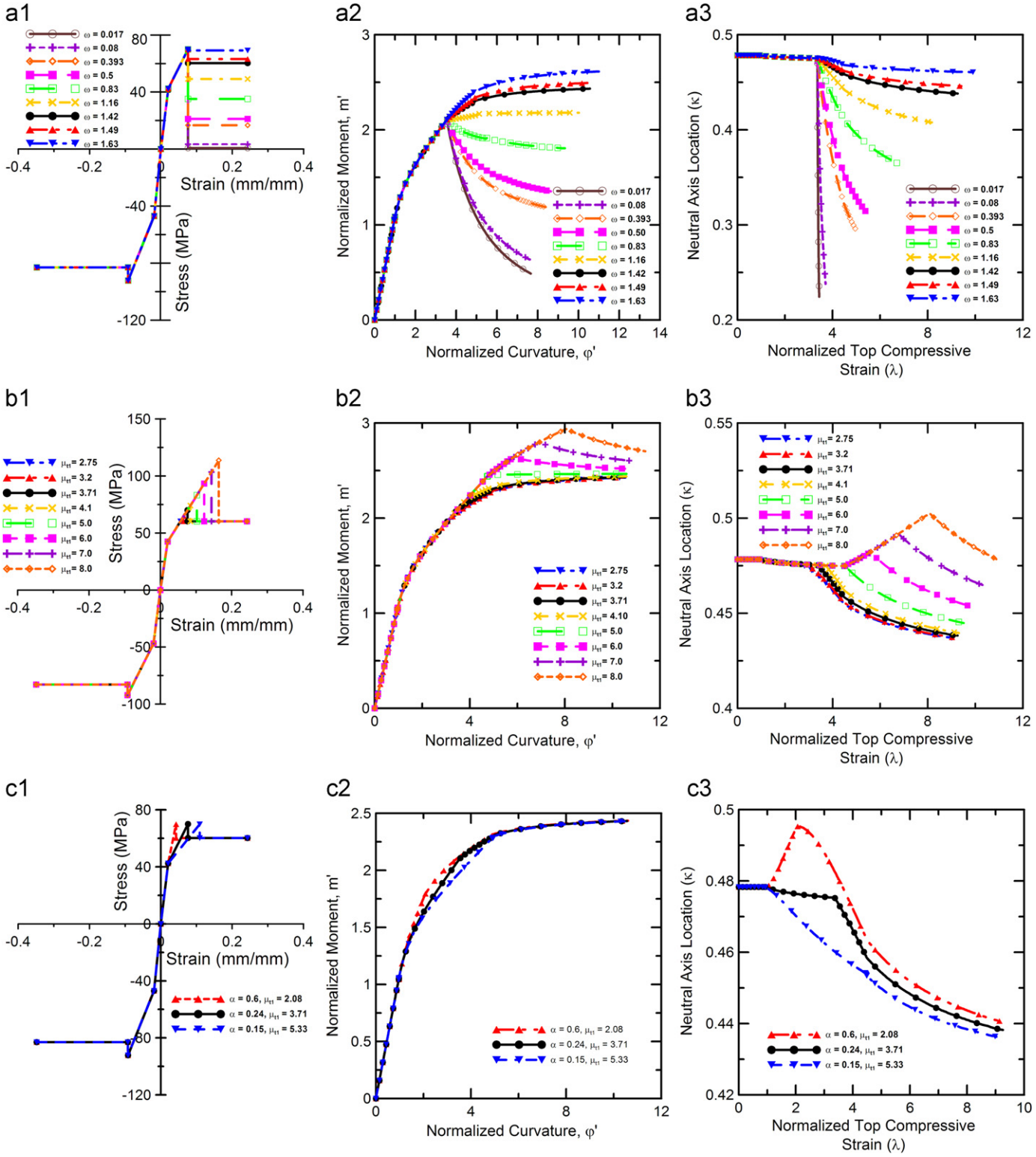

Fig. 4. Parametric study of a typical strain softening material.

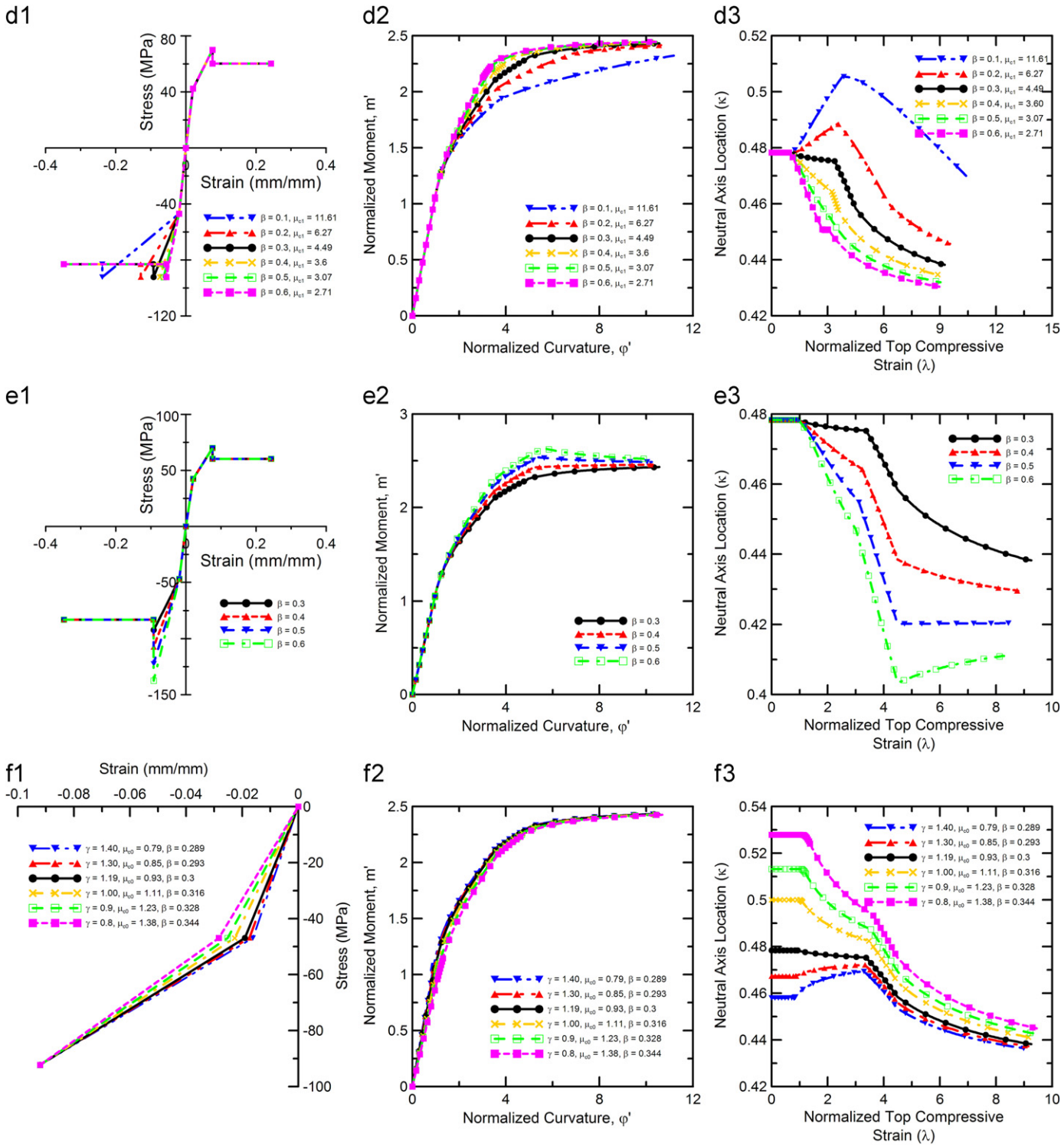

Fig. 4. (*continued*)

depends on the location and the history of the strain at that point. In this study, the length of the localized zone is 5 mm, thus the majority of the sections along the beam will undergo unloading. For the sections with moment less than the elastic moment, the curvature unloads elastically, while for the sections that have been loaded beyond elastic, the unloading curvature will depend on the recovery percentage of curvature, which can be taken as zero in the monotonic displacement control 3PB test. Knowing the curvature values along the beam for each load step, one can calculate the deflection at the mid-span for each load step using moment area method numerically [22]. The main steps to calculate load deflection response are summarized as following.

1. Calculate transition points to determine the possible cases of stress distribution based on material properties for a piecewise-linear model.

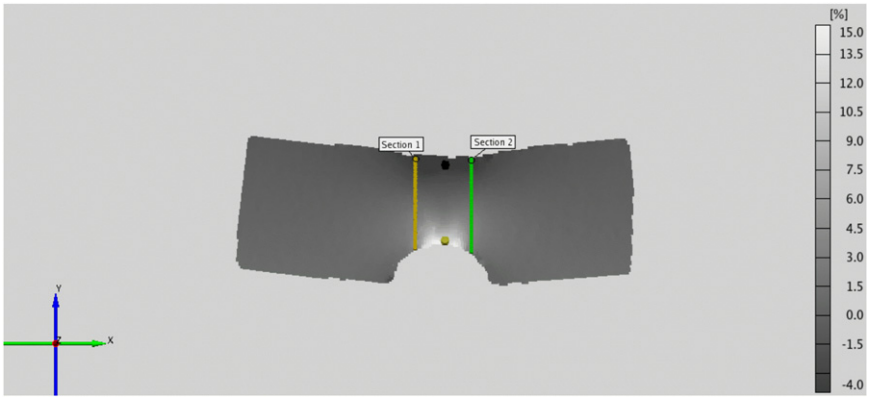

Fig. 5. Deformation localization area and longitudinal strain distribution at 493 μstr/s.

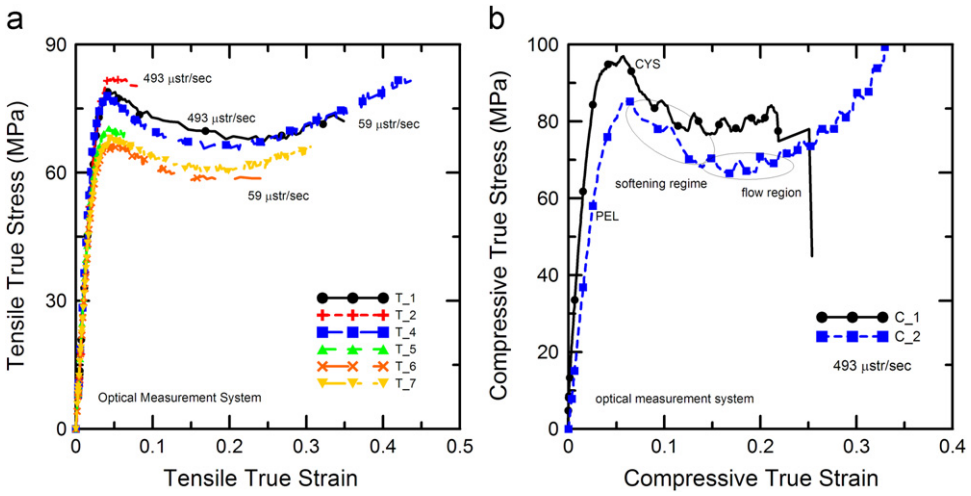

Fig. 6. (a) True stress–strain tension response; and (b)true stress–strain compression behavior.

2. Impose load incrementally by increasing the normalized top compressive strain to obtain the nonlinear moment curvature response.
3. Calculate the applied load vector ($P=2$ M/S where S is the span for the 3PB setup).
4. Calculate moment diagram for any load in step 3 along the beam.
5. Determine curvature diagram for any load in step 3 along the structure using moment curvature relationship, softening localizations, and the percentage of the curvature recovery.
6. Calculate the amount of deflection at the mid-span using moment area method.
7. Repeat steps 3–6 for each load.

6. Experiments

Tension, compression, and 3PB bending tests were conducted at room temperature and at low speed. An interface load cell (interface model SM-1000) was used to measure the axial load in all the tests. Digital image correlation technique (ARAMIS 4M) was used to study the strain fields. This technique recognizes the surface structure of the object to be measured in digital camera images and allocates coordinates to the image pixels. Stress–strain relationship could be found using this technique as it is capable of capturing loads off of the test machine and showing loads in the output file. Dog bone samples with a gage length of 14 mm and a rectangular cross section of 3.18 mm × 3.43 mm were selected to conduct the monotonic tensile tests. Small cubic samples (4 mm × 4 mm × 4 mm) were tested under monotonic compression at the rate of 493 μstr/s. Small beams with the width of 4 mm, thickness of 10 mm, and length of 60 mm with a groove in the middle of the beam were selected to conduct 3PB tests. Flexural tests were done with a speed approximately corresponding to axial strain rate of 493 μstr/s. Epoxy resin Epon E 863 with a hardener EPI-CURE 3290 using a 100/27 weight ratio was used. Fig. 6 illustrates the experimental true stress–strain curves from tension and compression tests. Through triggering between load cell and optical system and examining the strain field around the loading nose, load deflection responses from the 3PB tests were obtained. In tension and compression tests, vertical strain along the samples was calculated by taking the average of values of nine stage points located on a sign "+" in the highest strain region.

7. Flexural response of Epon E 863

Yekani Fard et al. [18,19] used a tension and compression strain softening stress and strain model, curve fitted to the experimentally-obtained-uniaxial stress–strain curves, to study the flexural response of E 863. While the compressive and tensile moduli are approximately equal for E 863, the elastic stress and the peak stress in tension are lower than those in compression. Therefore, E 863 does not experience compression plastic flow in bending and their stress–strain relationship in the compression

side is always in the ascending region and the first part of the softening regime, as shown by solid circles in Fig. 7 Therefore, a tension and compression stress–strain model with constant plastic flow stress (Fig. 1), might be more useful for modeling bending in epoxy resins, which are considerably stronger in compression than in tension. The tension and compression stress–strain response and the constant softening model for strain rate of 493 μstr/s are shown in Fig. 8(a). The mechanical properties of the constant softening model for 493 μstr/s are: $E=3049$ MPa, $\varepsilon_{PEL}=0.0162$, $\mu_{c0}=1.148$, $\mu_{c1}=3.52$, $\mu_{Uc}=15.70$, $\mu_{t1}=2.55$, $\mu_{Ut}=20.98$, $\gamma=1.09$, $\alpha=0.395$, $\beta=0.298$, $\omega=1.369$, and $\psi=1.62$.

Fig. 8(b) shows that the tension compression model under predicts the load deflection response. The main reasons for the under prediction is the difference between stress distribution profiles between uniaxial test and bending test. In tension and compression tests, the entire volume of the sample is subjected to the same load and has the same probability of failure. However, in a bending test, only a small fraction of the tension and compression regions is subjected to the maximum peak stress. Therefore, the probability of crack nucleation, propagation, and failure development in tension and compression samples is higher than the bending samples. Results of the parametric study show that flexural load carrying capacity can be improved by increasing the ultimate tensile and compressive levels through a flexural overstrength factor (parameter C_1) and by further adjustments to the other parameters. Fig. 9 shows the concept of the flexural overstrength factor. An inverse analysis technique of flexural results shows that C_1 is 1.25 for Epon E 863 at 493 μstr/s. The results from the analytical approach could be compared with the results from Weibull analysis approach [16,17] which estimated the mean flexural strength to be 40% higher than the tensile strength. More studies at different strain rates and on different epoxy resin materials need to be performed before an average flexural overstrength factor can be recommended.

8. Conclusions

Explicit moment curvature equations using nonlinear tension and compression stress–strain relation for epoxy resin materials have been developed. A multi-linear stress–strain relation for epoxy resin materials, consisting of constant post peak responses in tension and compression has been used. The material model is described by two intrinsic material parameters: (a) tensile modulus of elasticity and (b) tensile strain at the PEL point, in addition to six non-dimensional parameters for compression and four non-dimensional parameters for tension. A parametric study showed that the normalized moment–curvature response is primarily controlled by the normalized post peak tensile strength,

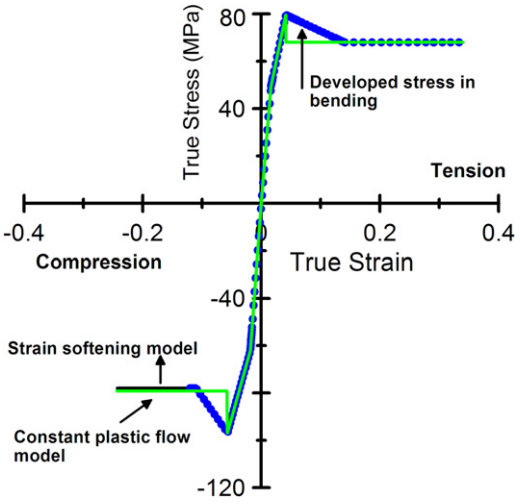

Fig. 7. Effect of compressive stress on flexural behavior at high strain values.

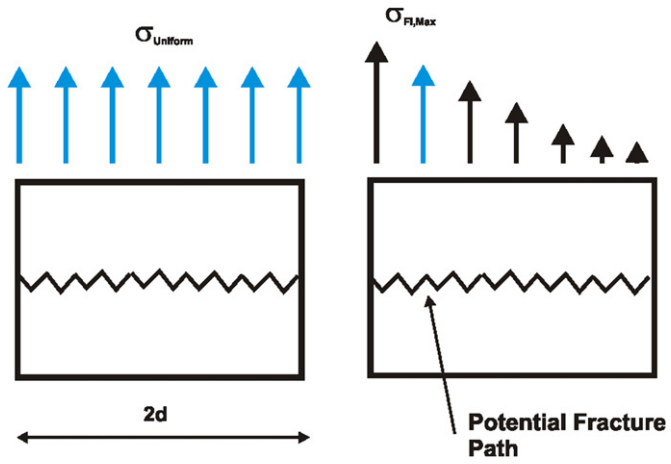

Fig. 9. Effect of stress gradient on maximum flexural strength.

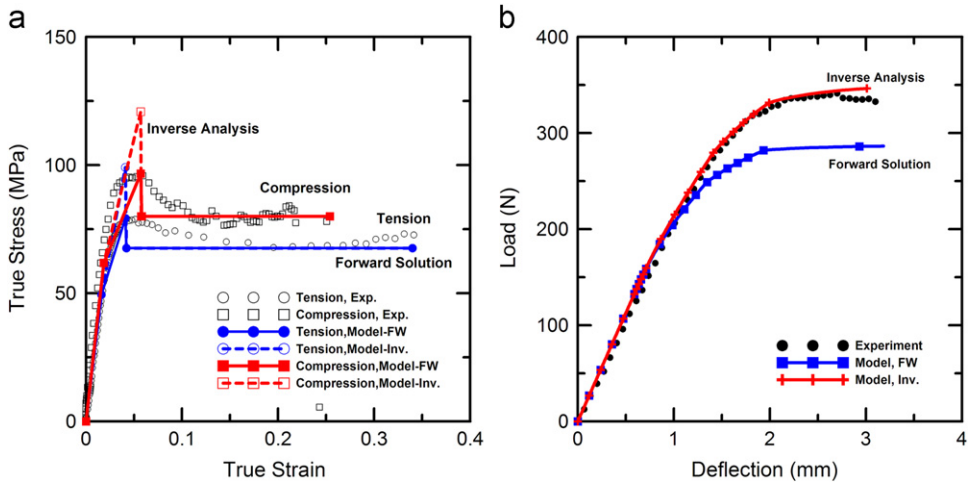

Fig. 8. (a) Experiment and simulation for tension and compression stress–strain curve at 493 μstr/s (b) simulation of load deflection for 3PB beam with groove at 493 μstr/s.

normalized UTS, and normalized CYS. Results show that materials with high normalized post peak tensile strength have a gradual reduction in the height of the compressive zone, therefore larger deformations are possible. Results show that while very brittle materials have a moment capacity equal to or less than the moment at PEL point, epoxy resin materials with a considerable amount of post peak tensile strength have a moment capacity around 2.5 times the moment at the PEL point. Increasing CYS by increasing the post compressive PEL stiffness at high CYS values marginally affects the moment capacity in polymeric materials. Simulation of the load deflection response of polymer materials in 3PB test revealed that direct use of tension and compression data under predicts the flexural response. Simulations of the experimental data clearly revealed the effect of stress gradient on the material behavior as the uniaxial tensile and compression tests yields a lower tensile and compression strength than the flexural tests. The prediction of flexural load carrying capacity can be improved by applying a flexural over-strength factor (C_1) to uniaxial tension and compression strength. The value of C_1 for Epon E 863 in 3PB beam with groove is estimated to be 1.25.

Acknowledgments

The authors gratefully acknowledge the support of this research by the Army Research Office, AMSRD-ARL-RO-SI proposal number: 49008-EG, agreement number: W911NF-07-1-0132, Program Manager: COL. Reed F. Young. We also thank Dr. Dallas Kingsbury from ASU for assistance in compressive, tension and bending tests.

References

[1] Wineman AS, Rajagopal KR. Mechanical Response of Polymers. New York: Cambridge Univeristy Press; 2000.
[2] Zhang C, Moore ID. Nonlinear mechanical response of high density polyethylene. II: Uniaxial constitutive model. Polym Eng Sci 1997;37:414–20.
[3] Li FZ, Pan J. Plane stress crack-tip fields for pressure sensitive dilatant materials. J Appl Mech 1990;57:40–9.
[4] Chang WJ, Pan J. Effects of yield surface shape and round-off vertex on crack-tip fields for pressure sensitive materials. Int J Solids Struct 1997;34:3291–320.
[5] Hsu SY, Vogler TJ, Kyriakides S. Inelastic behavior of an AS4/PEEK composite under combined transverse compression and shear, II: modeling. Int J Plast 1999;15:807–36.
[6] Gilat A, Goldberg RK, Roberts GD. Strain rate sensitivity of epoxy resin in tensile and shear loading. J Aerosp Eng, ASCE 2007:75–89.
[7] Jordan JL, Foley JR, Siviour CR. Mechanical properties of epon 826/DEA epoxy. Mech Time-Depend Mater 2008;12:249–72.
[8] Mulliken AD, Boyce MC. Mechanics of the rate-dependent elastic-plastic deformation of glassy polymers from low to high strain rates. Int J Solids Struct 2006;43:1331–56.
[9] Naaman AE, Reinhardt HW. Proposed classification of HPFRC composites based on their tensile response. Mater Struct 2006;39:547–55.
[10] Yekani Fard M, Liu Y, Chattopadhyay A. Nonlinear flexural behavior and moment curvature response of epoxy resin using digital image correlation technique. JMSE 2011;5:212–9.
[11] Yekani Fard M, Liu Y, Chattopadhyay A. Characterization of epoxy resin including strain rate effects using digital image correlation system. J Aerosp Eng, ASCE (2011) doi:10.1061/(ASCE)AS.1943-5525.0000127, (in press).
[12] Hobbiebrunken T, Fiedler B, Hojo M, Tanaka M. Experimental determination of the true epoxy resin strength using micro-scaled specimens. Compos Part A 2007;38:814–8.
[13] Bazant ZP, Chen E. Scaling of structural failure. Appl Mech 1997:593–627.
[14] Odom EM, Adams DF. Specimen size effect during tensile testing of an unreinforced polymer. J Mater Sci 1992;27:1767–71.
[15] Goodier JN. Concentration of stress around spherical and cylindrical inclusions and flaws. Trans Am Soc Mech Eng 1933;55:39–44.
[16] Giannotti MI, Galante MJ, Oyanguren PA, Vallo CI. Role of intrinsic flaws upon flexural behavior of a thermoplastic modified epoxy resin. Polym Test 2003;22:429–37.
[17] Vallo CI. Influence of load type on flexural strength of a bone cement based on PMMA. Polym Test 2002;21:793–800.
[18] Yekani Fard M, Liu Y, Chattopadhyay A. Analytical solution for flexural response of epoxy resin materials. J Aerosp Eng, ASCE (2011), doi:10.1061/(ASCE)AS.1943-5525.0000133, (in press).
[19] Yekani fard M, Liu Y, Chattopadhyay A. Inverse analysis of constitutive relation for epoxy resin materials. 52nd AIAA/ASME/ASCE/AHS/ ASC Structures, Structural Dynamics and Materials Conference, 4-7 April, Denver, Colorado, USA, 2011.
[20] Salmon CG, Johnson JE. Steel Structures: Design and behavior.3rd. ed. New York: Harper and Row; 1990.
[21] Littell JD, Ruggeri CR, Goldberg RK, Roberts GD, Arnold WA, Binienda WK. Measurement of epoxy resin tension, compression, and shear stress–strain curves over a wide range of strain rates using small test specimens. J Aerosp Eng 2008:162–73.
[22] Rajan SD. Introduction to structural analysis and design. John Wiley & Sons, Inc.; 2001.